72nd International Astronautical Congress (IAC), Dubai, United Arab Emirates, 25-29 October 2021.

IAC-21-C1.6.5-x65610

Ejecta dynamics around asteroids in view of in-orbit particle collection missions

Mirko Trisolini[a]*, Camilla Colombo[a], Yuichi Tsuda[b]

[a] *Department of Aerospace Science and Technology, Politecnico di Milano, via La Masa 34, 20156, Milano, Italy,* mirko.trisolini@polim.it
[b] *Institute of Space and Astronautical Science (ISAS)/Japan Aerospace Exploration Agency (JAXA),* 3-1-1 Yoshinodai, Chuo-ku, Sagamihara, Kanagawa 252-5210, Japan, tsuda.yuichi@jaxa.jp
* Corresponding Author

Abstract

This work explores the possibility of performing in-orbit particle collection for sampling and exploration missions towards asteroids. Ejecta is generated via a small kinetic impactor and two possible collection strategies are investigated: collecting the particle at the L_2 Lagrangian point or collecting them while the orbit the asteroid and before they re-impact. Combining the dynamics of the particles in the Circular Restricted Three-Body Problem with realistic models for the ejecta generation, we evaluate the feasibility of the mission concept and characterised possible target asteroids given their physical properties.

Keywords: asteroids, ejecta, sample collection, CR3BP

Acronyms/Abbreviations

CR3BP	Circular Restricted Three-Body Problem
SRP	Solar Radiation Pressure
NEA	Near Earth Asteroid
FOM	Figure of Merit
BLE	Ballistic Limit Equation
WCB	Weakly Cemented Basalt

1. Introduction

Space exploration missions to asteroids have always drawn the attention of the scientific and engineering community given the challenges they pose and the possibility they present to further our knowledge of the Solar System. Asteroids carry fundamental information on the evolution of our Solar System. They are rich in valuable resources such as metals, silicates, and water, which could be exploited through future asteroid mining missions, and enable long-duration mission self-sustaining. The physical composition of asteroids is varied and, in most cases, poorly understood; it can be significantly improved collecting and studying their samples. Improving our knowledge, we can better target asteroids to be exploited and increase the efficiency of asteroid deflection missions. Several missions have visited asteroids and other small bodies; however, only few have orbited, landed, or impacted on them. Examples are JAXA missions Hayabusa and Hayabusa2, ESA Rosetta, and NASA OSIRIS-REx. One of the most challenging aspects of such missions is to collect and sample asteroids material by means of an on-ground collection, involving landing (or touchdown) and mining.

In a context of future asteroid exploration missions, within the Collecting Asteroid-Orbiting Samples - CRADLE project, we envision the possibility to perform in-orbit collection as an alternative to landing or touchdown operations [1]. Such a collection mechanism relies on the knowledge of the dynamical behaviour of small particles orbiting the asteroid, which is influenced by the third body effect, solar radiation pressure and the gravitational potential of the asteroid. This paper explores the evolution of the small particles around asteroids in the context of the circular restricted three body problem. The ejection of the particles from the surface of the asteroid is obtained via a small kinetic impactor to obtain the distribution of the particles' ejection velocity and area-to-mass ratio.

While several previous works have studied the dynamical behaviour of small particles around asteroids and comets, these works have focused either on the long-term orbital evolution and the identification of families of quasi-stable orbits [2][3], usually neglecting the actual ejecta phenomenon, or on very specific targets [4][5], thus focusing on particular events.

In this work, instead, we aim at performing a general assessment of the problem at hand by combining the two fundamental contributions to understand the motion of impact-generated particles around small bodies: the dynamical behaviour after the impact and the generation of the initial conditions resulting from the impact event. With this general assessment we aim at identifying suitable targets for in-orbit particle collection missions. In this context, we analyse the feasibility of two possible scenarios for in-orbit particle collection missions. A first scenario that exploits the dynamical peculiarities of the

Lagrangian point L_2, where particles of given size and speed will tend to pass and produce favourable conditions for the collection. A second scenario that aims at collecting the particles orbiting the asteroid for a sufficient amount of time without re-impacting or escaping the neighbourhood of the asteroid. For both these scenarios, we study what targets properties are the best for an effective collection mission and what are the properties that, instead, lead to infeasible mission scenarios. To do so, we evaluate a Figure of Merit of the number of collectable particles for a given mission scenario.

2. Methodology

The first step towards the implementation of in-orbit particle collection missions consists of a feasibility study and a target selection analysis. Specifically, we want to answer the questions: can we collect asteroid samples resulting from the impact with a small kinetic impactor? If yes, what are the best types of targets to achieve such an objective? To answer these questions, it is fundamental to study the dynamics of the ejected particles around small bodies and to understand the impact phenomenon and the resulting properties of the ejected particles. In fact, combining the orbital dynamics of the samples with the physics of the ejecta generation is of critical importance to enable in-orbit particle collection missions. In the following section we will describe both the dynamical model and the ejecta model adopted in this study; we will highlight the relevant constraints and consequences related to cratering and impact dynamics, and we will outline the identified collection strategies.

2.1 Dynamical model

The dynamical model used in this work is the Circular Restricted Three-Body Problem (CR3BP) perturbed by solar radiation pressure (SRP). The choice of neglecting the gravitational perturbations, mainly J_2, directly follows the objectives of this work that is to have a general understanding of the phenomenon and of possible suitable targets. As the gravitational potential is accurately known only for few asteroids, this was considered a suitable assumption.

2.1.1 Solar radiation pressure effect

The effect of SRP is considered using a "cannon ball" model, where the ejected particles are considered spheres. In this case, the effect of SRP is conservative and the magnitude of its acceleration can be expressed as follows:

$$a_{SRP} = P_{SRP} \frac{S}{m} c_R \tag{1}$$

Where S is the cross-section exposed to the Sun, m is the mass and c_R is the reflectivity coefficient (0 for translucent particles, 1 for black bodies, and 2 for reflective particles). We can express the SRP acceleration as a function of a non-dimensional parameter, the lightness parameter β as follows:

$$a_{SRP} = \frac{\beta\, \mu_{Sun}}{r_{sp}^2} \hat{\boldsymbol{r}} \tag{2}$$

Where μ_{Sun} is the gravitational parameter of the Sun, r_{sp} is the Sun-to-particle distance and $\hat{\boldsymbol{r}}$ the Sun-to-particle direction. The lightness parameter can be expressed as:

$$\beta = \frac{P_0}{c} \frac{AU^2}{\mu_{Sun}} \frac{3 c_R}{2 \rho_p d_p} \tag{3}$$

Where $P_0 = 1367$ W/m^2 is the solar flux at 1 AU, c is the speed of light, AU is the astronomical unit, ρ_p is the particle density and d_p the particle diameter. The advantage of the cannon ball model is that we can express the SRP contribution as a potential as follows:

$$a_{SRP} = \nabla V_{SRP} \hat{\boldsymbol{r}}, \quad \text{where} \quad V_{SRP} = -\beta \frac{\mu_{Sun}}{r_{sp}} \tag{4}$$

2.1.2 Equations of motion

The equations of motion are expressed in non-dimensional form in a synodic reference frame centred in the asteroid.

$$\begin{cases} \ddot{x} - 2\bar{n}\dot{y} = V_{/x} \\ \ddot{y} - 2\bar{n}\dot{x} = V_{/y} \\ \ddot{z} = V_{/z} \end{cases} \tag{5}$$

Where x, y, and z are the non-dimensional particle positions with respect to the centre of the asteroid in the rotating frame, and $\bar{n}$ is the non-dimensional mean motion, equal to unity in this case. The potential V is expressed as follows:

$$V = \frac{1}{2}(x^2 + y^2) + (1-\mu)x + \frac{(1-\beta)(1-\mu)}{r_{sp}} + \frac{\mu}{r_{ap}} + \frac{1}{2}(1-\mu)^2 \tag{6}$$

With r_{sp} and r_{ap} the distances between the Sun and the particle and the asteroid and the particle, respectively.:

$$r_{sp} = \sqrt{(x+1)^2 + y^2 + z^2}$$
$$r_{ap} = \sqrt{x^2 + y^2 + z^2} \tag{7}$$

2.2 Ejecta model

The ejecta model describes the characteristics of the ejected particles after an impact that is the particle size, velocity, and launch direction. These quantities represent the initial conditions for the orbit propagation in the CR3BP. Specifically, we will use the ejecta model to describe the effect of an impact with a small kinetic

impactor, comparable to the one of the Hayabusa2 mission [6] (Fig. 1).

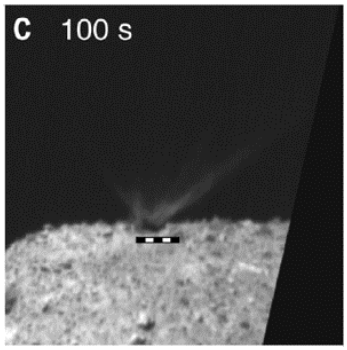

Fig. 1: Camera frame 100 seconds after the impact on the surface of asteroid Ryugu [6].

The ejecta model is defined using a density function of the form [7]:

$$\phi(s,u,\xi,\psi) = As^{-1-\alpha}u^{-1-\gamma}f(\xi)g(\psi) \tag{8}$$

Where s is the particle radius, u the ejection velocity, ξ the in-plane launch angle, and ψ the out-of-plane launch angle (measured with respect to the local horizontal frame centred at the impact location). The exponents α and γ regulate the slope of the distributions, while A is a scaling constant used for mass conservation. In the current implementation, the model considers an uncorrelated distribution where the size, velocity and launch direction of the particles are independent from each other [7][8]. We assume the ejection of the particle can be uniform withing a spherical sector so that the distribution functions for the launch direction can be expressed as:

$$f(\xi) = \begin{cases} \dfrac{1}{\xi_{max} - \xi_{min}} & \text{if } \xi_{min} \le \xi \le \xi_{max} \\ 0 & \text{elsewhere} \end{cases} \tag{9}$$

$$g(\psi) = \begin{cases} \dfrac{\cos(\psi)}{\sin(\psi_{max}) - \sin(\psi_{min})} & \text{if } \psi_{min} \le \psi \le \psi_{max} \\ 0 & \text{elsewhere} \end{cases} \tag{10}$$

The values of the minimum and maximum values of the launch angles can be selected. If we consider a perpendicular impact, we can expect an axisymmetric ejecta cloud so that ξ ranges from 0 to 360 degrees. The out-of-plane component of the launch angle (ejection angle) is usually limited. From experiments it has been observed an ejection angle usually ranging from 25 to 65 degrees [9]. In this work, this range is used.

The complete definition of the distribution function (Eq. (8)) requires the specification of additional quantities such as the minimum and maximum particle size. For this work, the minimum particle diameter is 10 μm, while the maximum is 10 cm. Additionally, the minimum and maximum ejection speed must be specified. To do so, we rely on experimental correlation for impacts and cratering events [10][11][12]. The ejection velocity can be expressed as a function of the impactor and target properties as follows:

$$\frac{u}{U} = C_1 \left[\frac{x}{a} \left(\frac{\rho}{\delta} \right)^{\nu} \right]^{-1/\mu} \tag{11}$$

Where U is the impactor speed, a is the radius of the impactor, ρ the target density, δ the impactor density, and C_1, μ, and ν are constants depending on the target material. The variable x is the radial distance from the impactor point. By substituting the minimum value $x_{min} = n_1 a$ (with n_1 = 1.2 [12]), we get the maximum ejection speed, while substituting the maximum value, equal to the crater radius, R, we get the minimum ejection speed. The crater radius can be computed as follows [12]:

$$\begin{aligned} R\left(\frac{\rho}{m}\right)^{1/3} &= H_2 \left(\frac{\rho}{\delta}\right)^{\frac{1-3\nu}{3}} \left[\frac{Y}{\rho U^2}\right]^{-\mu/2} && \text{stength} \\ R\left(\frac{\rho}{m}\right)^{1/3} &= H_1 \left(\frac{\rho}{\delta}\right)^{\frac{2+\mu-6\nu}{3(2+\mu)}} \left[\frac{ga}{U^2}\right]^{-\mu/(2+\mu)} && \text{gravity} \end{aligned} \tag{12}$$

Where the first expression is for an impact in the strength-dominated regime, while the second for a gravity-dominated regime. The parameter Y identifies the target strength, g the gravitational acceleration on the target surface, and m the impactor mass.

From a comparison between the ejecta distribution of Eq. (8) and the expression derived by Housen et al. [12], we can infer the expression for γ:

$$\gamma = 3\mu \tag{13}$$

Therefore, γ depends on the target material. The coefficient A can be obtained solving for the mass conservation as follows:

$$\int_{min}^{max} \phi(s,u,\xi,\psi)\, ds\, du\, d\xi\, d\psi = M \tag{14}$$

Where the mass ejected from the crater, M can be found as follows:

$$M = k\rho[x^3 - (n_1 a)^3] \tag{15}$$

Where k is again a constant depending on the target material.

An example of a 2D ejecta distribution in particle size and velocity is given in Fig. 2. The main features of the ejecta model can be observed: the particle density increases rapidly (it is a log-log plot) with decreasing ejection speed and particle size so that after an impact event the majority of the particles will be of small size and have low velocities.

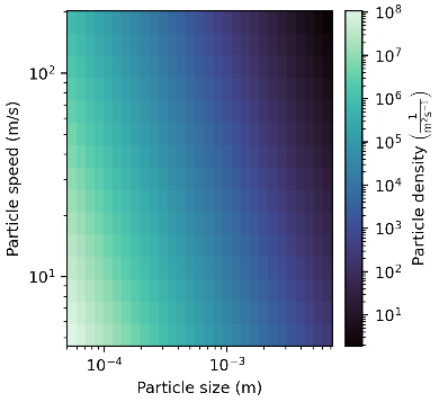

Fig. 2: Example of ejecta model distribution.

2.3 Preliminary collection evaluation

In this work, we present two possible strategies for in-orbit particle collection (Fig. 3).

1. Collecting the particles at the L_2 gap. This strategy has the advantage of knowing in advance where the particles will be, also as a function of their diameter (acting as a mass spectrometer). However, for the strategy to be interesting a sufficiently small gap should be considered, thus strongly limiting the feasible initial conditions of the ejecta for the L_2 passage.
2. Collecting the particles that will orbit the asteroid for enough time (to be defined based on operational constraints). This strategy has the advantage of having less constraints on the initial conditions of the ejecta. However, the particles will occupy the entire space around the asteroid and a more refined "collection trajectory" would be required for the spacecraft for an effective in-orbit collection.

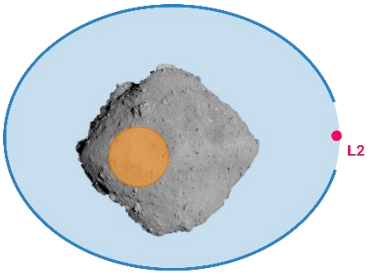

Fig. 3: Schematic representation of the collection areas. In orange the in-situ collection strategies; in cyan the orbiting collection region; in fuchsia the L_2 collection region.

As the objective of this work is to evaluate the feasibility of particle collection missions and identifying possible targets, it is necessary to evaluate a large combination of target characteristics, based on their density, dimensions, material type, and material strength. In fact, these parameters are the most influential in determining the properties of the ejecta plume.

At this point it is important to understand how effective the collection of samples can be for a given target. In this work, this is achieved by estimating the number of collectable particles given the target properties and the selected collection mechanism. The estimate of the number of particles is obtained exploiting the ejecta model described in Section 2.2, integrating the distribution of Eq. (8) for the ejection size, velocity, and direction intervals of interest.

The procedure is slightly different depending on the collection mechanism considered. Before going into the details of the procedures, we outline few common aspects for the analyses. Specifically, (a) the target analysis focuses on Near Earth Asteroids (NEAs), (b) the shape of the steroids is assumed to be spherical, and (c) the impactor characteristics are fixed. The implications of these assumptions are the following:

1. The computation of the SRP contribution is performed using an average value of the asteroid distance from the Sun that is the average semi-major axis of all catalogued NEAs that is equal to 1.755 AU.
2. The two quantities used in the analysis are the asteroid radius and density. The mass of the asteroids comes directly from
$$m_A = \frac{4}{3}\pi\rho_A r_A^3$$
3. No variation of impactor speed, density, or dimensions is currently considered. This allows having a general understanding of the mission feasibility. In addition, the impact outcome relevant to the in-orbit collection are not significantly influenced by the impactor properties [8]. The impactor properties are summarised in Table 1.

Table 1: Impactor properties.

Quantity	Symbol	Value
Speed (km/s)	U	2
Radius (m)	a	0.075
Density (g/cm^3)	δ	2.7

2.3.1 L_2-collection strategy

The L_2 collection strategy aims at exploiting the dynamical behaviour of those particles that tend to pass through the gaps that opens up in correspondence of the Lagrangian points given the right initial conditions. Typical analyses of trajectories at the Lagrangian points focus on the long-term dynamical behaviour and assume the initial conditions are given: however, the initial conditions strongly depend on the ejecta dynamics. Therefore, we analyse if the ejecta generated by a small

kinetic impactor can actually result in initial conditions leading to favourable collection scenarios at L_2. To do so, the underlying simplified procedure is followed:

1. Select a test particle of 1 mm in diameter
2. Compute the ejection velocity (u_{ej}) such that a "small gap" opens up at L_2, as follows [1]:

$$u_{ej} = u_{C2} + \epsilon \cdot (u_{esc} - u_{C2})$$

Where u_{esc} is the escape velocity from the asteroid, u_{c2} is the escape velocity associated to an energy C_2, equal to the Jacobi constant, and ε is a correction coefficient. In practice, the above expression defines an ejection velocity with an energy slightly bigger than C_2 so that we have a small gap at L_2.

3. Propagate a set of test trajectories (Fig. 5)

- Assuming a 2D CR3BP, we perform an ejection simulation from a point on the asteroid surface every 10 degrees in the first and fourth quadrant.
- For each point on the asteroid, a trajectory is simulated for a different ejection angle, with an interval of 5 degrees between 25 and 65 degrees.
- This is a total of 162 simulations for each combination of asteroid radius and density.

4. Estimate number of particles using ejecta distribution

To compute a Figure of Merit (FOM) that represents the availability of particles to be collected at L_2, we combine the simulations of point 3 with the ejecta distribution of Eq. (8). First, for each of the ejection location on the asteroid surface we identify the ejection velocity, and we estimate the number of particles they "carry" by integrating the ejecta distribution (e.g., Fig. 2) in a neighbourhood of the ejection conditions defined by particle size and ejection speed as follows:

$$n_{p,i} = \iint_{s_0,u_0}^{s_1,u_1} \phi(s,u)\, ds\, du \tag{16}$$

With $\phi(s,u)$ is the particle number density only as a function of particle size and speed. Since the distribution is considered uniform in the ejection direction, for each ejection location the particle number $n_{p,i}$ is scaled with the fraction of trajectories passing through L_2 (red lines in Fig. 4). The figure of merit is then the average over all the ejection locations as follows:

$$FOM_{L2} = \log_{10}\left[\frac{1}{M}\cdot\sum_{i=1}^{M}\frac{n_{L2,i}}{N}\cdot n_{p,i}\right] \tag{17}$$

Where M is the number of ejection locations, N the total number of trajectories propagated from each ejection location and $n_{L2,i}$ the number of trajectories passing through L_2.

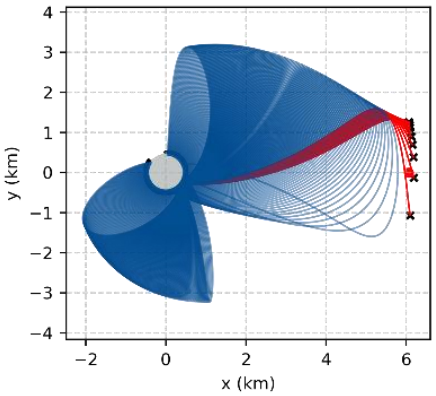

Fig. 5: Example of trajectories following an impact event. In red the trajectories passing through L_2.

2.3.2 Orbiting collection strategy

For the orbiting collection strategy, we consider collectable all those particles that orbit the asteroid for enough time before re-impacting the asteroid surface.

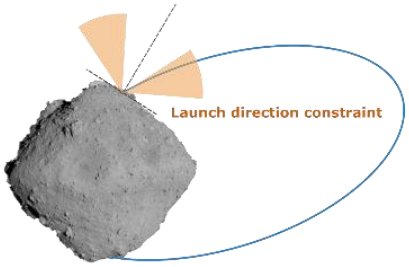

Fig. 6: Schematics of the keplerian motion followed by the particles re-imapcting the aseroid. This particles can collected before re-impact. In orange the range of possible ejection angles.

To understand the feasibility and quality of the collection we estimate the number of collectable particles. We follow a simple approach as described below:

1. Specify a particle size range: 0.1 – 2 mm
2. Select a range of ejection velocities (Fig. 7):
   - Simplified Keplerian motion
   - Minimum speed, u_{min}, from the minimum time before re-impact: 3 hours in this analysis
   - Maximum speed, u_{max}, from the maximum time before re-impact: 3 days in this analysis

3. Propagate the trajectories as in Section 2.3.1
   - Grid in ejection location every 45°
   - Grid in launch angles: between 25° and 65°
4. Identify the percentage of trajectories still orbiting for a time greater than t_{MIN} = 3 hours
5. Estimate number of particles and compute the Figure of Merit (FOM_{orb})
   - Integrate ejecta distribution in the selected ranges
   - Weight the distribution with the previous percentage

$$FOM_{orb} = \log_{10}\left[\sum_{k=0}^{n_d}\left(\int_{s_k}^{s_{k+1}}\int_{u_{min}}^{u_{max}} w_k \phi(s,u)\, ds du\right)\right] \quad (18)$$

Where n_d is the number of bins in which we divide the particle diameter range and w_k is the weight representing the percentage of particles still orbiting. As the diameter influences the dynamical behaviour, different fractions of particles will still be orbiting as a function of their dimensions. Therefore, each contribution is weighted differently.

3. Results

We present here the results of the analyses performed following the methodology of Section 2.3. The main objective of the paper is to address the feasibility of in-orbit collection for specific targets. This objective is achieved combining the effects of realistic impact conditions, modelled as described in Section 2.2, with the dynamics of small particles perturbed by SRP. It is important at this point to remember that the composition of most asteroids is still unknown, leading to a considerable uncertainty when it comes to predicting their density and soil strength. As these parameters have a strong influence on the outcome of the ejecta model, it is critical to perform a parametric analysis considering different material types and strength levels.

In the following, we take into account two materials commonly used in modelling asteroid's soil [5][9][12]: *sand* and *weakly cemented basalt* (WCB). The first material is representative of very loose soil with strength close to zero: therefore, they are used to model gravity-dominated impacts. The second material is representative of weakly cohesive soils, similar to regolith [11]. The material properties relative to the ejecta model formulation are summarised in Table 2.

Table 2: Ejecta model material properties.

	Sand	WCB
μ	0.41	0.46
C_1	0.55	0.18
k	0.3	0.3
H_1	0.59	-
H_2	-	0.38
n_1	1.2	1.2
Y (MPa)	0	0.45
A (Eq. (8))	2	2.7

The analysis considers a range of possible asteroid sizes and densities. Specifically, the radius of the asteroid varies from 100 m to 15 km, while the asteroid density from 1 g/cm^3 to 5.3 g/cm^3. The radius range derives from data in the NASA asteroid small body database, excluding small objects. The density ranges are derived from average densities of common asteroid spectral classes [13].

3.1 Sand-like material

The first material considered is a sand-like soil. For this type of material, we have a gravity-dominated impact that is characterised by a wide range of ejection velocities. Given the negligible strength level, the minimum ejection speed is always smaller than the escape speed of the asteroids considered. Fig. 8 shows the results for the L_2 collection mechanism.

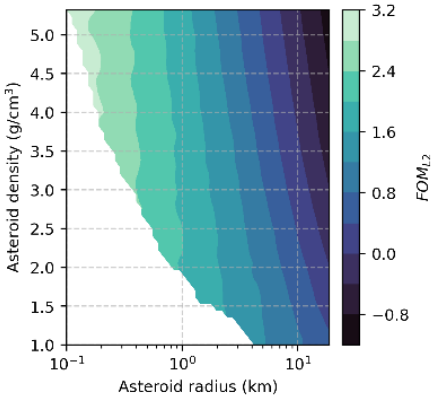

Fig. 8: L_2 collection FOM for a sand-like material.

We can observe that the highest FOM is achieved for targets with small radii and high densities. This can be explained looking simultaneously at the ejecta model and the consequence of having small asteroids. Small asteroids require low velocities for the L_2 passage. Looking at the ejecta model, low velocities are associated with higher particle densities and, thus, higher figure of merit. Another notable feature of Fig. 8 is the white bottom-left portion. This area represents infeasible solutions that is no test particle could reach the L_2 point for the given target characteristics.

Fig. 9 shows an equivalent plot for the orbiting collection strategy. In this case, there are no infeasible solutions and particles are predicted to be available for collection for all types of targets. Also, a similar trend for the FOM can be observed, with lower values for large and denser asteroids. The peak value of the FOM is instead in the bottom left corner, where small and less dense asteroids reside.

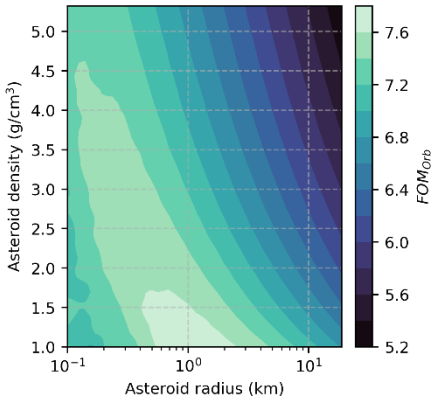

Fig. 9: Orbiting collection FOM for a sand-like material.

3.2 Weekly cohesive material

This second test case focuses on more cohesive materials, comparable to regolith. The considered material is the Weakly Cemented Basal, which has already been used to model the ejecta behaviour of the Deep Impact mission on comet Temple 1 [9] and for the Asteroid Impact & Deflection Assessment (AIDA) mission [4][5].

As for Section 3.1, we present the results for both the L_2 collection and the orbiting collection option. As for these types of materials also the assumed strength, *Y*, is important, we present here the results for an intermediate value equal to 10 kPa. This value is lower than the one reported in Table 2; however, it is considered to be more representative of possible asteroid soils as they tend to be weaker. Richardson et al. [9] found 10 kPa to be a reasonable value for the soil strength of comet Temple1, the strength of lunar regolith is estimated between 1 and 3 kPa [10], and the impact on asteroid Ryugu showed a very weak soil, with an impact almost fully gravity dominated.

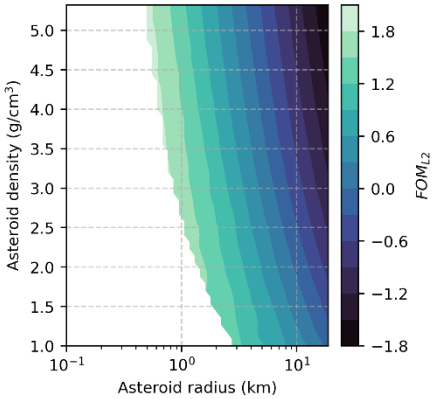

Fig. 10: L_2 collection FOM for WCB.

Despite the small amount of data available, the one we possess supports the assumption of a low soil strength. Considering this assumption, Fig. 10 and Fig. 11 show the computed figure of merit for the L_2 and orbiting collection strategies, respectively. A first interesting feature is the size and shape of the feasibility region. For both strategies, the infeasibility region is similar as in this case it is dominated by the minimum ejection velocity (Eq. (11)), which is dominated by the material strength. Differently from the sand-like material, in this case, the infeasibility region is present because all the ejected particles have a velocity greater than the escape velocity of the asteroid. The infeasibility region in Fig. 10 is only marginally larger as in this case some solutions are not feasible because of the L_2 passage constraint.

As for Section 3.1, the most favourable conditions, within the feasibility area, are for small radii and high densities for the L_2 collection, and for small radii and low densities for the orbiting collection. In Fig. 11 we can also identify a maximum in the bottom left part of the feasibility region, which was not visible in Fig. 9.

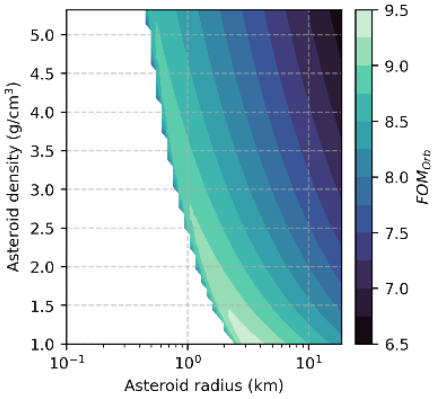

Fig. 11: Orbit collection FOM for WCB.

3.3 Target selection analysis

A preliminary target search among catalogued Near-Earth Asteroids (NEAs) is given in this section, for both the L_2 and *Orbital* collection solutions. The analysis is based on the Figure of Merit as described in the previous sections and on the reachability of the asteroids. The reachability is simply evaluated estimating the required Δv for the mission. The method used is the one outlined by Shoemaker and Helin [15]. We used the NASA Small-Body Database[1] to retrieve asteroids' orbital, dimensions, and composition information. The results shown here only consider "named" asteroids, with an estimated diameter already present in the NASA database. Density information is derived from the spectral class of the asteroid according to [13].

[1] https://ssd.jpl.nasa.gov/tools/sbdb_query.html

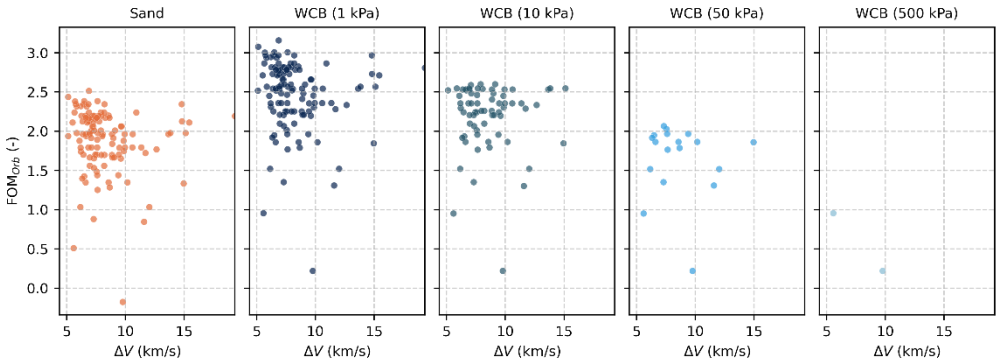

Fig. 12:

Fig. 12 shows the results for the L_2 collection mechanism for a test particle of 0.5 mm. Each plot has on the x-axis the Δv required for the mission and on the y-axis the FOM. The different sub-plots show different material types and strengths. Specifically, we considered Sand-like material, Weakly Cemented Basalt with four different strength levels. Several targets have been identified even at varying strength levels for a more robust selection mechanism. The last case, with a high specific strength material, only offers two solutions. We can also observe that several options are available even at the lower end of the delta-v range, thus ensuring the feasibility of the mission. Fig. 13 summarises the number of possible targets depending on the material type and strength.

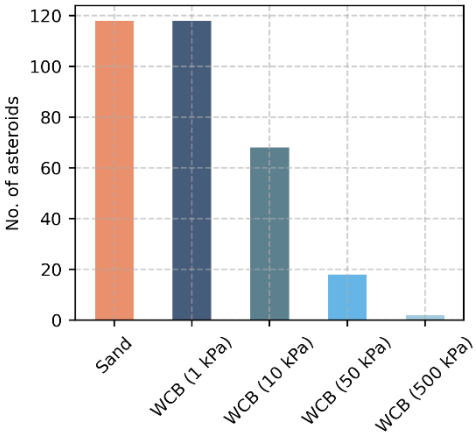

Fig. 13: Number of identified targets for L_2 collection as function of target material. Test particle: 0.5 mm size.

Similarly, Fig. 15 shows the required delta-v and the FOM for the Orbital collection strategy as a function of the target material and strength. A similar trend can be identified. In particular, the same targets are present for the WCB case at the highest strength level. Fig. 14 shows the total number of identified targets as function of the material, which shows a trend like Fig. 13: Sand-like and low-strength WCB would guarantee more options for the target selection.

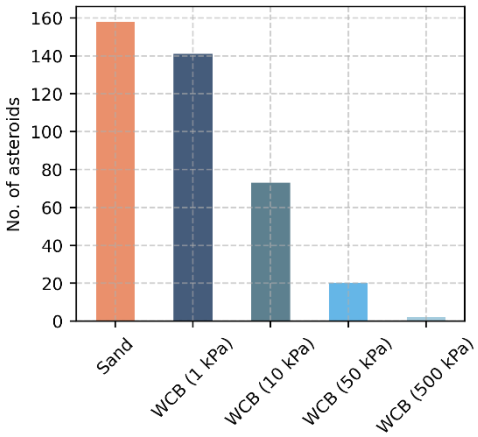

Fig. 14: Number of identified targets for the Orbital collection strategy as function of target material.

3.4 Preliminary risk analysis from particles impacts

To assess the feasibility of the mission it is also necessary to verify that the impact of the particles with the spacecraft is not dangerous such that the mission can be compromised. For this assessment, we model the impact of the orbiting particle s with the spacecraft using Ballistic Limit Equations (BLEs) [14], which have been extensively used to evaluate the risk posed by space debris on objects orbiting the Earth [16].

For the purpose of this study, a simplified approach has been followed. We consider a single-wall BLE for ballistic impacts (below the hypervelocity limit) as follows:

$$d_c = \left[\frac{\frac{1}{K_{3S}} \cdot t_w^{0.5} \cdot \left(\frac{\sigma_y}{40}\right)^{0.5}}{0.6 \cdot (\cos\theta)^{\delta} \rho_p^{0.5} u_p^{2/3}} \right]^{18/19} \quad (19)$$

Where d_c is the critical diameter that is the minimum diameter required to damage the single wall plate of thickness t_w if hit by a particle of density ρ_p and velocity

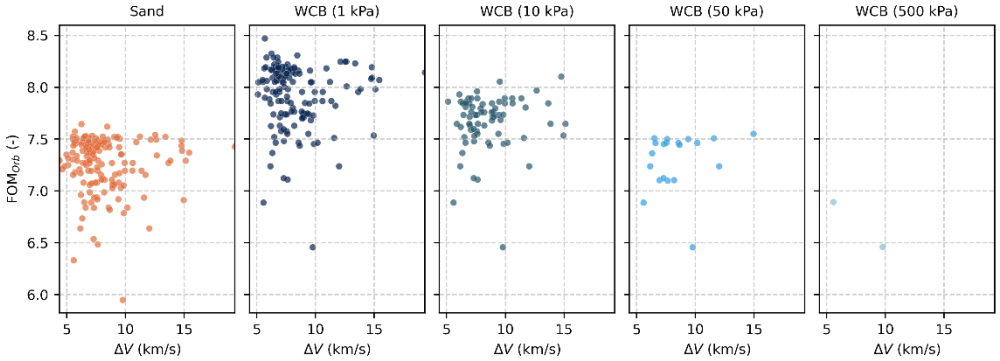

Fig. 15:

u_p. For the case in exam, we consider an aluminium plate with tensile strength σ_y = 276 MPa (to be converted in ksi for use in Eq. (19)) and a normal impact (θ = 0 deg). The parameters K_{3S} = 1.4 and δ = 4/3 are associated to impacts on aluminium plates.

Combining the ejecta distribution of Eq. (8) with the information of the BLEs, we can estimate which ejected particles can be dangerous for the spacecraft that is all particles with a diameter larger than the critical diameter predicted by Eq. (19). Fig. 16 and Fig. 17 show the variation of the ratio between the particle diameter and the critical diameter for the ejecta distributions relative to sand-like material and WCB, respectively.

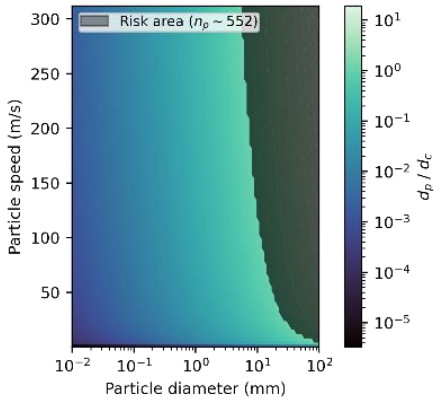

Fig. 16: Ratio between particle diameter and critical diameter for sand-like materials. Black shaded area: risk region.

In both cases we can observe a black shaded region concentrated in the upper right portion of the plot that identifies potentially dangerous particles. In this case the particle diameter is greater than the critical one. As expected, the bigger the particle the more likely is to cause damage even at smaller velocities. We can also observe that the sand-like material (Fig. 16) has a larger risk area since the ejection velocities are higher than the WCB case. In addition, by combining the shaded area of Fig. 16 and Fig. 17 with the particle density distribution (equivalent to Fig. 2), we can estimate the number of dangerous particles for both cases.

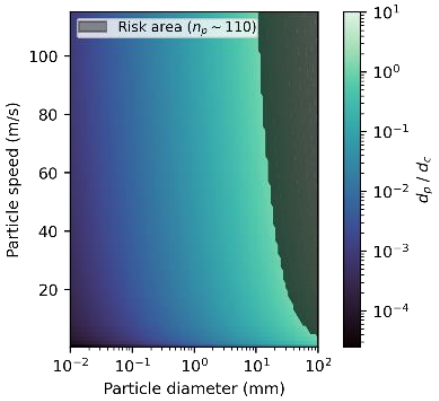

Fig. 17: Ratio between particle diameter and critical diameter for WCB material. Black shaded area: risk region.

We can observe that a sand-like material generates five time the dangerous particles of WCB, with about 550 risky fragments. This number of particles has to be put in perspective, since the total amount of particles generated by such an impact is of the order of 10^7-10^9 depending on the target/impactor combination.

4. Conclusions and discussion

In this work, we performed a preliminary analysis of the feasibility of in-orbit particle collection missions considering two collection scenarios: at the L_2 point and orbiting around the asteroid. For both scenarios, feasibility regions have been identified considering relevant characteristics of the target (i.e., the asteroid radius and density). The analyses have been performed also considering uncertain parameters such as the material type and the material strength of the asteroid. Specifically, sand-like and weakly cemented basalt have been considered. From the results, the orbiting collection option seems favoured by sand-like materials as no infeasible regions can be identified. A similar behaviour instead is observed for the weakly cemented basalt.

However, it has to be noted that the analysis for the orbiting option is simplified and does not consider the contribution of SRP. Further analyses, in line with the ones of the L_2 option should be carried out for a better assessment of this collection option.

For both the collection options, a Figure of Merit has been developed for a preliminary assessment of the collection capabilities as function of the target properties. In fact, the FOM is directly related to an estimate of the collectable particles. The results shows that both collection options can be more efficient for smaller asteroids; however, the L_2 option favours denser targets, while the orbiting options less dense ones. Another interesting aspect is the substantial difference between the magnitudes of the FOMs of the two options for both materials. The orbiting option tend to have FOM three to five times larger than the L_2 option. This behaviour can be expected as the conditions for collection at L_2 are far more restrictive. Additionally, the L_2 FOM only considers a single test diameter while the other considers a range of values.

Finally, a preliminary assessment of the risk the ejected particles pose to the spacecraft showed that few particles (in the order of hundreds) can be dangerous. This is quite a small value, compared to the total number of fragments generated by an impact. Moreover, the performed analysis is conservative as a 1 mm single-wall configuration has been analysed. More common options, such as honeycomb sandwich panels can offer a greater protection and further reduce the risk for the spacecraft.

Acknowledgements

This project has received funding from the European Union's Horizon 2020 research and innovation programme under the Marie Sklodowska-Curie grant agreement No 896404 – CRADLE.

References

[1] Latino, A., Soldini, S., Colombo, C., & Tsuda, Y. (2019). Ejecta orbital and bouncing dynamics around asteroid Ryugu. In *70th International Astronautical Congress (IAC 2019)*.

[2] Villegas-Pinto, D., Soldini, S., Tsuda, Y., & Heiligers, J. (2020). Temporary Capture of Asteroid Ejecta into Periodic Orbits: Application to JAXA's Hayabusa2 Impact Event. In *AIAA Scitech 2020 Forum* (p. 0221).

[3] Soldini, S., & Tsuda, Y. (2017). Assessing the hazard posed by Ryugu ejecta dynamics on Hayabusa2 spacecraft. In *26th International Symposium of Space Flight Dynamics*.

[4] Yu, Y., & Michel, P. (2018). Ejecta cloud from the AIDA space project kinetic impact on the secondary of a binary asteroid: II. Fates and evolutionary dependencies. *Icarus*, *312*, 128-144.

[5] Yu, Y., Michel, P., Schwartz, S. R., Naidu, S. P., & Benner, L. A. (2017). Ejecta cloud from the AIDA space project kinetic impact on the secondary of a binary asteroid: I. mechanical environment and dynamical model. *Icarus*, *282*, 313-325.

[6] Arakawa, M., Saiki, T., Wada, K., Ogawa, K., Kadono, T., Shirai, K., ... & Miura, A. (2020). An artificial impact on the asteroid (162173) Ryugu formed a crater in the gravity-dominated regime. *Science*, *368*(6486), 67-71.

[7] Sachse, M., Schmidt, J., Kempf, S., & Spahn, F. (2015). Correlation between speed and size for ejecta from hypervelocity impacts. *Journal of Geophysical Research: Planets*, *120*(11), 1847-1858.

[8] Trisolini M., Colombo C., Tsuda Y., "Ejecta analysis for an asteroid impact event in the perturbed circular restricted three body problem," *31st JAXA Workshop on Flight Mechanics and Astrodynamics*, Virtual, 26-27 July 2021.

[9] Richardson, J. E., Melosh, H. J., Lisse, C. M., & Carcich, B. (2007). A ballistics analysis of the Deep Impact ejecta plume: Determining Comet Tempel 1's gravity, mass, and density. *Icarus*, *191*(2), 176-209.

[10] Holsapple, K. A., & Housen, K. R. (2007). A crater and its ejecta: An interpretation of Deep Impact. *Icarus*, *191*(2), 586-597.

[11] Holsapple, K. A., & Housen, K. R. (2012). Momentum transfer in asteroid impacts. I. Theory and scaling. *Icarus*, *221*(2), 875-887.

[12] Housen, K. R., & Holsapple, K. A. (2011). Ejecta from impact craters. *Icarus*, *211*(1), 856-875.

[13] Carry, B. (2012). Density of asteroids. *Planetary and Space Science*, *73*(1), 98-118.

[14] Ryan, S., Christiansen, E.L., 2010. Micrometeoroid and orbital debris (MMOD) shield ballistic limit analysis program. Technical ReportNASA/TM-2009-214789. Houston.

[15] Shoemaker, E. M., & Helin, E. F. (1978). Earth-approaching asteroids as targets for exploration. Asteroids: An exploration assessment, 245-256.

[16] Trisolini M., Lewis H.G., Colombo C., "Predicting the vulnerability of spacecraft components: modelling debris impact effects through vulnerable-zones," *Advances in Space Research*, 2020, Vol. 65, Issue 11, pp. 2692-2710, DOI: https://doi.org/10.1016/j.asr.2020.03.010